Inorganic Chemistry

Communication

pubs.acs.org/IC

Structure Change Induced by Terminal Sulfur in Noncentrosymmetric $La_2Ga_2GeS_8$ and $Eu_2Ga_2GeS_7$ and Nonlinear-Optical Responses in Middle Infrared

Mei-Chun Chen,[†,‡] Peng Li,[†] Liu-Jiang Zhou,[†,‡] Long-Hua Li,[†] and Ling Chen*[,†]

[†]Key Laboratory of Optoelectronic Materials Chemistry and Physics, Fujian Institute of Research on the Structure of Matter, Chinese Academy of Sciences, Fuzhou, Fujian 350002, People's Republic of China

[‡]Graduate University of Chinese Academy of Sciences, Beijing 100039, People's Republic of China

Supporting Information

ABSTRACT: Two new noncentrosymmetric quaternary sulfides, $La_2Ga_2GeS_8$ (**1**) and $Eu_2Ga_2GeS_7$ (**2**), have been synthesized by high-temperature solid-state reactions. The structure change on going from **1** to **2** to the known $Li_2Ga_2GeS_6$ (**3**) nicely shows that the reduced cation charge-compensation requirement causes a decrease in the number of terminal S atoms per formula, which is a key to determining the connectivity of the GaS_4 and GeS_4 building units. Powder sample **2** exhibits a strong second-harmonic-generation (SHG) response of about 1.6 times the benchmark $AgGaS_2$ at 2.05 μm laser radiation, a non type I phase-matchable behavior, and a comparable transparency region. The SHG intensities of these compounds originate from the electronic transitions from S 3p states to La/Eu/Li−S, Ga−S, and Ge−S antibonding states according to Vienna ab initio simulation package studies.

Chalcogenides with tetrahedrally coordinated metal centers have attracted considerable interest because of not only their diverse structural features but also their useful physical properties, such as second-order nonlinear-optical (NLO) properties.[1] The examples include $AgGaS_2$,[1d,2] $AgGaGeS_4$,[3] $LiGaS_2$,[4] $BaGa_4S_7$,[5] $Li_2Ga_2GeS_6$,[6] and Li_2CdMS_4.[7] Among them, $AgGaS_2$ is the well-known middle-infrared (mid-IR) benchmark NLO material exhibiting a high second-harmonic-generation (SHG) coefficient, a wide transparent range, etc. However, the low-laser-damage threshold of this material limits its application.[2] Also, most of the reported IR NLO crystals are still in the experimental stage. Thus, the design and development of new materials with excellent NLO performance are of great importance.

An interesting noncentrosymmetric (NCS) β-$LaGaS_3$ phase made by GaS_4 building units shows a weak SHG effect.[8] The NCS compound Sm_4GaSbS_9 featuring a novel three-dimensional (3D) network constructed by asymmetric Sb_2S_5 and dimeric GaS_4 building units displays strong SHG responses.[9] In this Communication, the discoveries of $La_2Ga_2GeS_8$ (**1**) and $Eu_2Ga_2GeS_7$ (**2**) with SHG response will be reported; **2** shows a strong intensity of approximately 1.6 times that of $AgGaS_2$. The structure change and the role of the cation on the band gap as well as the origin of the SHG intensity are discussed.

Two new NCS quaternary sulfides, light-yellow **1** with a yield of about 50% and orange **2** with a yield of 70%, were synthesized from La/Eu, Ga, Ge, and S elements by solid-state reactions. The byproducts in **1** were difficult to identify, and that in **2** was centrosymmetryic ternary $Eu_2Ga_2S_4$. Numerous efforts to synthesize a single phase failed (see the Supporting Information, SI). Properties were measured on samples ground from handpicked crystals. As shown in Figure S1 in the SI, after such a treatment, **1** still mixed with ∼10% of an ambiguous phase and **2** still contained ∼5% of $EuGa_2S_4$. Both compounds were stable in air for several months.

Compound **1** crystallizes in the NCS orthorhombic space group $Cmc2_1$ with its own type, whereas **2** adopts a $Ca_2Ga_2GeO_7$-type structure in the NCS tetragonal space group $P\bar{4}2_1m$.[10] Both structures consist of stacking layers of connected GaS_4 and GeS_4 tetrahedral building units with La^{3+} or Eu^{2+} cations locating between the layers (Figure 1a,b). However, their building units are connected in different ways. The 2D $[Ga_2GeS_8]^{6-}$ layers in **1** are constructed by wavy GaS_4 chains that are interconnected by individual GeS_4 tetrahedra via sharing S apexes in a manner in which each GeS_4 tetrahedron has two terminal S apexes (μ_t-S) and each GaS_4 tetrahedron holds only one μ_t-S apex (Figures 1a and 2a), Differently, 2D $[Ga_2GeS_7]^{4-}$ layers in **2** are fabricated by $(GaS_4)_2$ dimers linked by individual GeS_4 tetrahedra. In this case, all apexes of the GeS_4 tetrahedron act as μ_2-S that is shared with neighboring $(GaS_4)_2$ dimers, while each GaS_4 has one μ_t-S and three μ_2-S apexes (Figures 1b and 2b). Interestingly, the layer in **1** is reminiscent of that in a related known orthorhombic 3D compound $Li_2Ga_2GeS_6$ (**3**), in which the wavy GaS_4 chains are interconnected in a similar manner on the *ab* plane but differently along the *c* direction, roughly along which each GaS_4 extends also as a chain, and eventually, the 3D $[Ga_2GeS_6]^{2-}$ framework is constructed[6] (Figure 1c). Both the terminal and bridging S atoms per formula can be calculated through the following function: $2n_{\mu_2\text{-S}} + n_{\mu_t\text{-S}} = 12$, where $n_{\mu_2\text{-S}}$ or $n_{\mu_t\text{-S}}$ is the number of bridging or terminal S atoms. We can deduce that $n_{\mu_2\text{-S}} = 6$ and $n_{\mu_t\text{-S}} = 0$ for **3**, $n_{\mu_2\text{-S}} = 5$ and $n_{\mu_t\text{-S}} = 2$ for **2**, and $n_{\mu_2\text{-S}} = 4$ and $n_{\mu_t\text{-S}} = 4$ for **1**. These calculated results are identical with the single-crystal analysis results. In accordance with the

Received: September 20, 2011
Published: November 16, 2011

   dx.doi.org/10.1021/ic2020513 | *Inorg. Chem.* 2011, 50, 12402−12404

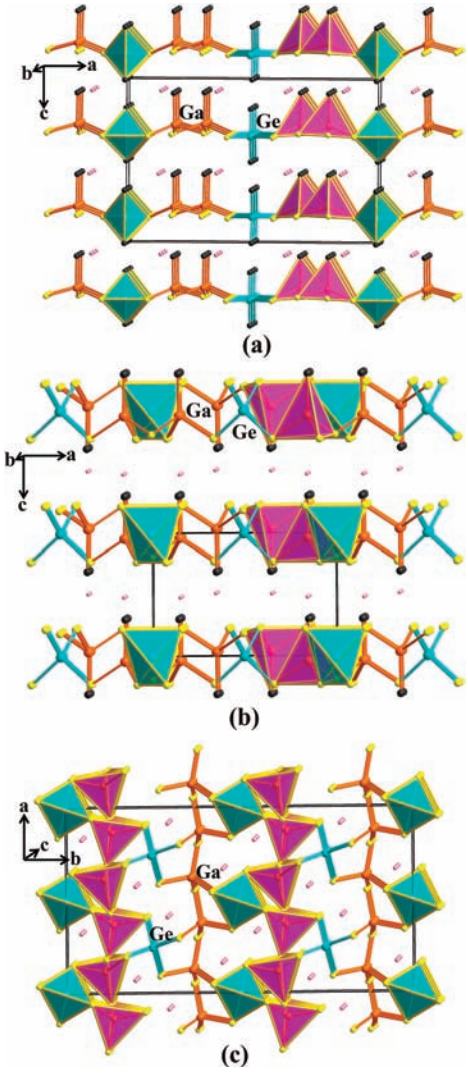

Figure 1. Structures of (a) **1**, (b) **2**, and **3** with unit cells outlined: yellow, μ_2-S; black, μ_t-S; orange, Ga; light green, Ge; pink, $La^{3+}/Eu^{2+}/Li^+$. Light-green tetrahedra: GeS_4. Pink tetrahedra: GaS_4.

electrostatic valence sum rule, **1**–**3** are all charge-balanced, $(La^{3+})_2(Ga^{3+})_2Ge^{4+}(S^{2-})_8$, $(Eu^{2+})_2(Ga^{3+})_2Ge^{4+}(S^{2-})_7$, and $(Li^+)_2(Ga^{3+})_2Ge^{4+}(S^{2-})_6$, respectively. Note that these compounds contain the same number of A, Ga, and Ge atoms per formula and only differ in the number of S^{2-} anions, which originates from the different cation charge-balance requirement. More interestingly, the number of μ_t-S apexes is a key to determining the many ways that GaS_4 and GeS_4 tetrahedra can be joined to build the crystal structure. The empirical structure indicators, M/r,[11] are 0.5, 0.67, and 1 for **1**–**3**, respectively (Table S4 in the SI). As the M/r value increases, the aggregation density of the anionic moiety (ADAM) increases.

Distortions of GaS_4 and GeS_4 tetrahedra in both compounds are indicated by the bond and angle deviations from the ideal ones. The Ga–S bonds and S–Ga–S angles in **1** and **2** are [2.237(3)–2.289(2) Å, 104.0–120.2°] and [2.168(3)–2.271(2) Å, 95.8–122.1°], whereas the Ge–S bonds and S–Ge–S angles are [2.187(4)–2.255(2) Å, 90.4–115.0°] and [2.257(2) Å, 101.5–113.6°]. In general, the distortion of GaS_4 is greater than that of GeS_4.

The La^{3+} cation in **1** (CN = 8) centers a distorted bicapped trigonal prism, whereas Eu^{2+} (CN = 6) is in a trigonal

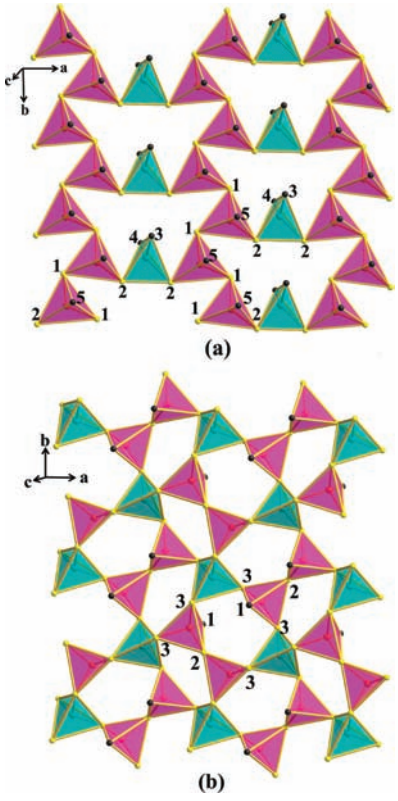

Figure 2. Layers of (a) **1** and (b) **2** with S atoms numbered: yellow: μ_2-S; black, μ_t-S. Light-green tetrahedra: GeS_4. Pink tetrahedra: GaS_4.

antiprism, while Li^+ (CN = 4) is tetrahedrally coordinated[6] (Figure S3 in the SI). La–S = 2.93–3.12 Å and Eu–S = 2.93–3.11 Å are in good agreement with the reported values of La_3CuGeS_7 (2.87–3.17 Å) and $EuGa_2S_4$ (3.05–3.13 Å).[12]

Compound **2** exhibits paramagnetic behavior over 2–300 K (Figure S4 in the SI) according to the Curie–Weiss law with C = 15.5 cm^3 mol^{-1} K and θ = 0.07. The measured effective magnetic moment $\mu_{eff} = (8C)^{1/2}$ = 7.87/Eu μ_B agrees well with the theoretical value for the isolated ground-state Eu^{2+} ion (7.9 μ_B) obtained from the equation $\mu_{eff} = g[J(J+1)]^{1/2}$,[13] which confirms the 2+ valence state for Eu and no magnetic coupling between Eu^{2+} centers (Eu–Eu = 4.22 Å).

More interestingly, powder samples **1** and **2** show the SHG response to 2.05 μm laser radiation. The SHG intensity of **1** is weak, and that of **2** is approximately 1.6 times the benchmark $AgGaS_2$ at a particle size of 46–74 μm. In comparison with those of $AgGaS_2$, **2** exhibits a non type I phase-matchable behavior (Figure S7 in the SI), a relatively smaller band gap (2.30 vs 2.56 eV; Figure S5 in the SI), a similar transparent range (0.65–21 vs 0.6–23 μm; Figure S6 in the SI), and a larger static birefringence (0.098 vs 0.039). The measured and calculated linear and NLO parameters for **1**–**3** are summarized in Table 1 (more details in the SI).

The calculated band gaps for **1**–**3** are 1.88, 1.70, and 2.36 eV, respectively. These are comparable with the experimental data (2.78, 2.30, and 3.65 eV; Figure S5 in the SI). The tops of the valence bands (VBs) of these compounds are primarily dominated by the S 3p states, but the components of the bottoms of the conduction bands (CBs) are different. In the CB-1 regions in **1**–**3**, the contributions of the S 3p, Ge 4s, and S 3s states are similar and are respectively as follows (%): S 3p, 35, 47, 55; Ge 4s, 25, 30, 33; S 3s, 9, 8, 7. However, the

dx.doi.org/10.1021/ic2020513 | *Inorg. Chem.* 2011, 50, 12402–12404

Table 1. Optical Properties of 1 and 2 Compared with Those of 3 and $AgGaS_2$ (AGS)

	1	2	3	AGS
SHG coefficient (pm/V) at 2.05 μm[b]	d_{33} = 25.27	d_{36} = 16.18	d_{33} = 3.85	d_{36} = 18.21
	d_{24} = 2.77		d_{24} = 2.44	
	d_{15} = 0.24		d_{15} = 13.13	
absorption edge (μm)	$0.62_{(obs)}$[a]	$0.65_{(obs)}$[a]	$0.34_{(obs)}$[6]	$0.60_{(obs)}$[a]
	$0.46_{(cal)}$	$0.53_{(cal)}$	$0.34_{(cal)}$	$0.46_{(cal)}$
transmn range (μm)	NA	0.65−21[a]	NA	0.60−23[a]
band gap (eV)	$2.78_{(obs)}$[a]	$2.30_{(obs)}$[a]	$3.65_{(obs)}$[6]	$2.56_{(obs)}$[a]
	$1.88_{(cal)}$[b]	$1.70_{(cal)}$[b]	$2.36_{(cal)}$[b]	2.70[2b]
static birefringence[b]	0.077	0.098	0.004	0.039
average refractive index at 2.05 μm[b]	2.803	2.466	2.383	2.489
average static dielectric ions[b]	7.786	6.032	5.647	6.149

[a]Measured on powdered crystals. [b]Calculated (more details in the SI).

contributions of cations in the same region are significantly distinct, for example, La 5d contributes 19% (Figure S17 in the SI), Eu 5d 9% (Figure S18a), and Li 2p 0% (Figure S19 in the SI). Accordingly, the optical absorptions for **1** and **2** can be mainly ascribed to the charge transitions from the S 3p states to the Ge 4s, La 5d/Eu 5d, and S 3s states, but that for **3** is from the S 3p states to the Ge 4s and S 3s states. Obviously, rare-earth cations narrow the band gap, but Li does not, which well explains the band gap decrease from **3** to **1**/**2**.

Cutoff-energy-dependent SHG coefficients of **2** shown in Figure S18b reveal that the overall SHG coefficient is mainly determined by two regions, VB-1 and CB-3. The major character of VB-1 is the S 3p states (~87%). Also, those of CB-3 are 53% Eu 5d states together with 21% S 3p, 11% Ga 4p, and 4% Ge 4p states. Therefore, the overall SHG efficiency should be influenced by the S 3p, Eu 5d, Ga 4p, and Ge 4p states. Similar contributions are found in **1**: VB-1, 87% S 3p states; CB-3, 35% La 5d, 33% S 3p, 15% Ga 4p, and 7% Ge 4p states (Figure S17 in the SI). Also, those in **3** are as follows: VB-1, 90% S 3p states; CB-3, 17% Li 2p, 37% S 3p, 23% Ga 4p, and 8% Ge 4p states (Figure S19 in the SI). Consequently, the major SHG response comes from the electronic transitions from the S 3p states to the La/Eu/Li−S, Ga−S, and Ge−S antibonding states.

In conclusion, two new mid-IR NLO-active quaternary semiconductors **1** and **2** are discovered. The nice structure change from **1** to **2** to **3**[6] is induced by the different cation charge-balance requirement. The number of terminal S atoms per formula is a key to determining the linkage of GaS_4 and GeS_4 building units as well as ADAM. Theoretical analyses reveal that rare-earth cations narrow the band gaps but Li does not, whereas all components influence the SHG response via the electronic transitions from the S 3p states to the La/Eu/Li−S, Ga−S, and Ge−S antibonding states. This understanding may shed useful light on further explorations and predesign syntheses of new NLO compounds. Interestingly, powder sample **2** shows a strong SHG response of about 1.6 times the benchmark $AgGaS_2$ at 2.05 μm, a non type I phase-matchable behavior, a comparable transparent range, and larger static birefringence. The growth of large crystals for further physical property studies is worth pursuing.

■ ASSOCIATED CONTENT

Supporting Information

CIF data, experimental and theoretical methods, and additional tables and figures. This material is available free of charge via the Internet at http://pubs.acs.org.

■ AUTHOR INFORMATION

Corresponding Author

*E-mail: chenl@fjirsm.ac.cn.. Tel: (011)86-591-83704947.

■ ACKNOWLEDGMENTS

This research was supported by the National Natural Science Foundation of China under Projects 90922021, 20733003, 20973175, 21171168, and 21103190 and the "Knowledge Innovation Program of the Chinese Academy of Sciences" (KJCX2-YW-H20 and CXJJ-11-M71).

■ REFERENCES

(1) (a) Sheldrick, W. S.; Wachhold, M. *Coord. Chem. Rev.* **1998**, *176*, 211. (b) Mitchell, K.; Ibers, J. A. *Chem. Rev.* **2002**, *102*, 1929. (c) Liao, J. H.; Marking, G. M.; Hsu, K. F.; Matsushita, Y.; Ewbank, M. D.; Borwick, R.; Cunningham, P.; Rosker, M. J.; Kanatzidis, M. G. *J. Am. Chem. Soc.* **2003**, *125*, 9484. (d) Nikogosyan, D. N. *Nonlinear optical crystals: a complete survey*; Springer-Science: New York, 2005.

(2) (a) Harasaki, A.; Kato, K. *Jpn. J. Appl. Phys.* **1997**, *36*, 700. (b) Jayaraman, A.; Narayanamurti, V.; Kasper, H. M.; Chin, M. A.; Maines, R. G. *Phys. Rev. B* **1976**, *14*, 3516.

(3) Petrov, V.; Badikov, V.; Shevyrdyaeva, G.; Panyutin, V.; Chizhikov, V. *Opt. Mater.* **2004**, *26*, 217.

(4) Isaenko, L.; Yelisseyev, A.; Lobanov, S.; Krinitsin, P.; Petrov, V.; Zondy, J. J. *J. Non-Cryst. Solids* **2006**, *352*, 2439.

(5) Lin, X. S.; Zhang, G.; Ye, N. *Cryst. Growth Des.* **2009**, *9*, 1186.

(6) Kim, Y.; Seo, I.-s.; Martin, S. W.; Baek, J.; Halasyamani, P. S.; Arumugam, N.; Steinfink, H. *Chem. Mater.* **2008**, *20*, 6048.

(7) Lekse, J. W.; Moreau, M. A.; McNerny, K. L.; Yeon, J.; Halasyamani, P. S.; Aitken, J. A. *Inorg. Chem.* **2009**, *48*, 7516.

(8) Li, P.; Li, L. H.; Chen, L.; Wu, L. M. *J. Solid State Chem.* **2010**, *183*, 444.

(9) Chen, M. C.; Li, L. H.; Chen, Y. B.; Chen, L. *J. Am. Chem. Soc.* **2011**, *133*, 4617.

(10) Belokoneva, E. L.; Belov, N. V. *Dokl. Akad. Nauk SSSR* **1981**, *260*, 1363.

(11) Wu, L. M.; Wu, X. T.; Chen, L. *Coord. Chem. Rev.* **2009**, *253*, 2787.

(12) (a) Poduska, K. M.; DiSalvo, F. J.; Min, K.; Halasyamani, P. S. *J. Alloys Compd.* **2002**, *335*, L5. (b) Roques, R.; Rimet, R.; Declercq, J. P.; Germain, G. *Acta Crystallogr., Sect. B* **1979**, *35*, 555.

(13) (a) Kahn, O. *Molecular Magnetism*; VCH Publishers: New York, 1993. (b) van Vleck, J. H. *The Theory of Electric and Magnetic Susceptibilities*; Oxford University Press: Oxford. U.K., 1932.